RSC Advances

PAPER

View Article Online
View Journal | View Issue

Cite this: *RSC Adv.*, 2023, **13**, 21211

An insight into the hydrogen bonding, halogen bonding and chalcogen bonding interactions in manganese(III) complexes with N_2O_2donor salicylidine Schiff base ligands†

Mridul Karmakar,[a] Wahedur Sk,[a] Rosa M. Gomila,[b] Michael. G. B. Drew,[c] Antonio Frontera *[b] and Shouvik Chattopadhyay *[a]

Four manganese(III) complexes, $[MnL^1(H_2O)_2]ClO_4 \cdot H_2O$ (**1**), $[MnL^2(H_2O)_2]ClO_4$ (**2**), $[MnL^3(DMSO)(H_2O)]ClO_4$ (**3**) and $[MnL^4(DMSO)(H_2O)]ClO_4$ (**4**), where H_2L^1 = *N*,*N*′-bis(5-bromosalicylidene)-1,3-diaminopropane, H_2L^2 = 2,2-dimethyl-*N*,*N*-bis(3-methyloxysalicylidene)-1,3-diaminopropane, H_2L^3 = *N*,*N*′-bis(5-chlorosalicylidene)-2,2-dimethyl-1,3-diaminopropane and H_2L^4 = 2-hydroxy-*N*,*N*′-bis(3-ethyloxysalicylidene)-1,3-diaminopropane are tetradentate N_2O_2-donor ligands and DMSO = dimethyl sulfoxide, have been synthesized and characterised by elemental analysis, IR and UV-vis spectroscopy and single-crystal X-ray diffraction studies. All are monomeric complexes. Complex **1** crystallises in orthorhombic space group $P2_12_12_1$, complex **3** crystallises in triclinic space group *P*-1, whereas complexes **2** and **4** crystallize in monoclinic space groups, *C*2/*c* and *C*2/*m* respectively. In all the complexes, manganese(III) has a six-coordinated pseudo-octahedral geometry in which imine nitrogen atoms and phenolate oxygen atoms of the deprotonated di-Schiff base constitute the equatorial plane. In complexes **1** and **2**, water molecules are present in the fifth and sixth coordination sites in the axial positions while in complexes **3** and **4** they are occupied by one water and one DMSO. The coordinated water molecules initiate hydrogen-bonded networks in all complexes. DFT calculations have been carried out to analyze two aspects of these complexes *viz.* the formation of halogen (HaB) and chalcogen bonding (ChB) interactions in complexes **1** and **3** where the electron donor is the perchlorate anion and the acceptor either bromine or chlorine atoms for the HaBs and the sulfur atom of the coordinated DMSO for the ChB. In addition, other intermolecular effects are discussed in the solid state for complexes **1**, **2** and **4**, where the hydrogen atoms of the coordinated water molecules interact with the electron rich cavities formed by the phenolate and alkyloxy oxygen atoms of the Schiff-base ligand.

Received 15th June 2023
Accepted 3rd July 2023

DOI: 10.1039/d3ra04044e

rsc.li/rsc-advances

Introduction

Synthetic inorganic chemists have used several salen type N_2O_2-donor Schiff base ligands to form varieties of manganese(III) complexes.[1–6] The complexes are usually octahedral, where the tetradentate H_2 salen-type ligand occupies four coordination sites and other appropriate co-ligands occupy the axial sites. It is well established that the four donor atoms (two nitrogens and two oxygens) of the salen ligand around the metal centre can assume two different arrangements: (i) all imine and phenolate donor atoms occupy the equatorial positions (favoured by the presence of two monodentate ligands),[7–17] and (ii) one oxygen atom is displaced from the equatorial plane, occupying an axial position of the coordination polyhedron (favoured by the presence of a bidentate chelating ligand).[7,18–23] In this work, we shall concentrate on the first type arrangement, where $[Mn^{III}$(Schiff base)$]^+$ cations (with a high spin state) may have a strong uniaxial magnetic anisotropy created by the Jahn–Teller effect in an octahedral ligand field.[24] In some complexes, the axial sites are filled by water molecules and these complexes may be utilized for the construction of several water bridged complexes. These complexes may also be important in understanding the mechanism of ligand replacement reactions. In these complexes, the hydrogen atoms of the coordinated water molecules will also be involved in hydrogen bonding.[25]

[a]*Department of Chemistry, Jadavpur University, Kolkata-700032, West Bengal, India. E-mail: shouvik.chattopadhyay@jadavpuruniversity.in*

[b]*Departamento de Química, Universitat de les IllesBalears, Crta.deValldemossakm 7.5, 07122 Palma, Baleares, Spain. E-mail: toni.frontera@uib.es*

[c]*School of Chemistry, The University of Reading, P. O. Box 224, Whiteknights, Reading RG6 6AD, UK*

† Electronic supplementary information (ESI) available. Figures from S1–S9, Cif of complexes **1–4**. CCDC 2260214–2260217 for complexes **1–4**, respectively. For ESI and crystallographic data in CIF or other electronic format see DOI: https://doi.org/10.1039/d3ra04044e

Obviously, the most commonly used approach for engineering the supramolecular structure of these complexes is to utilize hydrogen bonds. However, many other non-covalent interactions, such as, π-stacking, cation–π, C–H···π, lone-pair···π, anion···π, hydrophobic interactions, *etc.*, are also important for the synthesis and the stabilization of the different supramolecular architectures of the complexes. Recently, σ-hole interaction involving a positive electrostatic potential region (called an σ-hole, created by the anisotropic distribution of the electron density) and an electron rich center of the molecule is widely studied and has been found relevance in stabilizing the supramolecular assemblies. σ-Hole interactions involving group 6, 7 and 8 metals are called osme bonds, wolfium bonds and matere bonds respectively.[26] Such interactions are called spodium bonds and tetrel bonds for group 12 and group 14 elements respectively.[27] The non-covalent interactions involving the elements of halogen and chalcogen groups are called halogen bonding (HaB) and chalcogen bonding (ChB) interactions respectively.[28–30]

In the present work, we have used 1,3-diaminopropane moiety to prepare some salen-type Schiff base ligands, which have, in turn, been used to synthesize a series of mononuclear manganese(III) complexes. In each of the complexes, the imine nitrogen atoms of the Schiff bases form six-membered chelate rings with the manganese(III) centers, see Scheme 1.

The DFT study is utilized to analyze the formation of recurrent motifs in the solid state of complexes consisting of supramolecular dimers where the hydrogen-atoms of the coordinated water molecules interact with the electron rich cavity formed by the phenolic and alkyloxy oxygen atoms of the Schiff-base ligand, as detailed in the following sections. We have also rationalized the formation of halogen bonding and chalcogen bonding interactions in complexes, where the electron donor is the perchlorate anion and the acceptor either bromine or chlorine atoms for the HaBs and the sulfur-atom of the coordinated DMSO for the ChB, see Scheme 2. In particular compound **1** forms infinite chains of perchlorate anions bridges by lattice water molecules with appended Mn(III) complexes where bifurcated halogen bonds are establishes (see Scheme 2A). Moreover, compound **3** forms infinite 1D chains where the cationic Mn(III) complexes are interconnected by the perchlorate anions that forms concurrent halogen and chalcogen bonds (see Scheme 2B). As all four complexes are cationic with perchlorate counter anions, the potential energy density at the bond CP has also been calculated to estimate the strength of the bifurcated HaB free from the pure coulombic attraction between the counter ions.

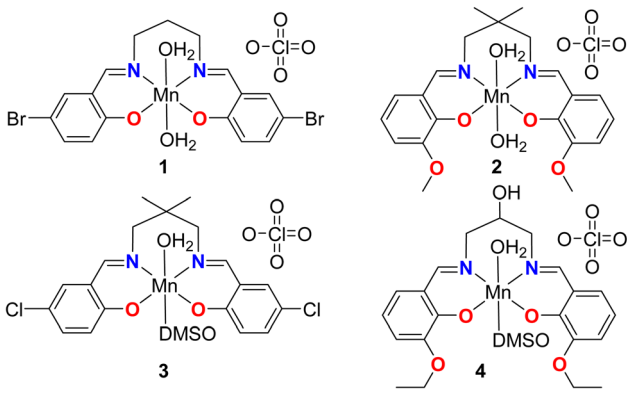

Scheme 1 Manganese complexes **1–4** reported in this work.

Experimental

The starting ingredients and solvents utilized in the experiment were all of reagent-grade quality, readily available, and procured from Sigma-Aldrich. Without any further purification, all of them were used for experiments.

Synthesis

Synthesis of $[MnL^1(H_2O)_2]ClO_4 \cdot H_2O$ (1). 5-bromosalicyldehyde (0.402 g, ~2 mmol) and propane-1,3-diamine (0.10 mL, ~1 mmol) were refluxed at a 2 : 1 molar ratio in 10 mL methanol for around 4 hours. Then the solution was cooled down to room temperature and a methanol/water (4 : 1) solution (5 mL) of manganese(II) perchlorate hexahydrate (0.362 g, ~1 mmol) was

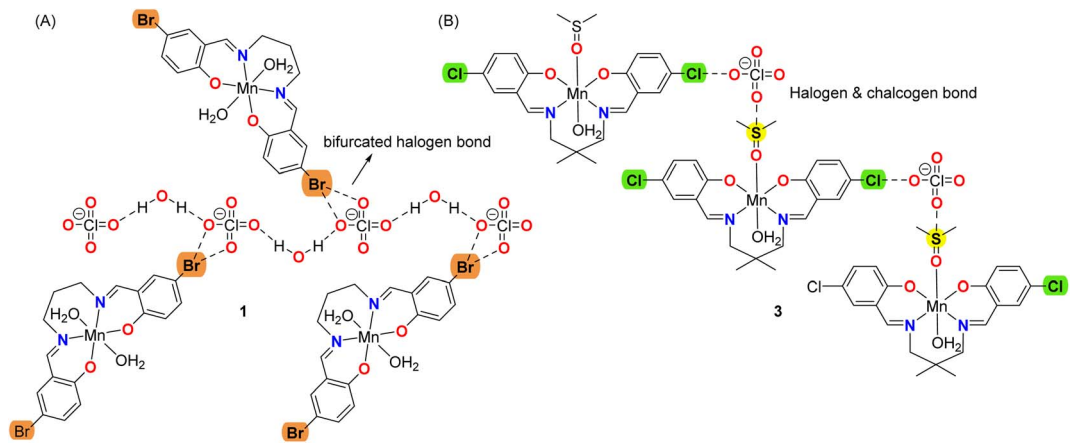

Scheme 2 Representation of the halogen bonding interactions in **1** and concurrent halogen and chalcogen bonds in **3**.

added to it with constant stirring. The yellow colour of the solution turned into dark brown. After 1 h, the resulting solution was filtered and the solution was kept undisturbed. Deep brown, blocked-shaped, single crystals of **1**, suitable for X-ray diffraction, were obtained after a few days by slow evaporation of the resulting solution in an open atmosphere. It was re-crystallized from methanol solution.

Complex **1**: yield: 401 mg (∼62%). Calc. for $C_{17}H_{20}Br_2ClMnN_2O_9$ (FW 646.55): C, 31.58; H, 3.12; N, 4.33%. Found: C, 31.57; H, 3.14; N, 4.35%. FT-IR (KBr, cm^{-1}): 1610 ($\nu_{C=N}$); 2948 (ν_{C-H}); 3364 (ν_{O-H}). UV-vis, λ_{max} (nm), [ε_{max} (L mol^{-1} cm^{-1})] (CH_3CN), 221 (3.4×10^4), 275 (1.8×10^4), 377 (5.8×10^3), 579 (1.5×10^3). Magnetic moment = 5.02 B. M. HRMS (ESI, positive ion mode, acetonitrile) *m*/*z*: 492.7210 (cald. 493.06) for $[Mn(L^1)]^+$.

Synthesis of $[MnL^2(H_2O)_2]ClO_4$ (2). Complex **2** was synthesized in a similar technique using 3-methoxysalicyldehyde (0.304 g, ∼2 mmol) and 2,2-dimethylpropane-1,3-diamine (0.13 mL, ∼1 mmol), instead of 5-bromosalicyldehyde and propane-1,3-diamine respectively. X-ray-quality single crystals were obtained after 9–10 days on slow evaporation of the reaction mixture in an open atmosphere. It was re-crystallized from methanol solution.

Complex **2**: yield: 364 mg (∼65%). Calc. for $C_{21}H_{28}ClMnN_2O_{10}$ (FW 558.84): C, 45.13; H, 5.05; N, 5.01%. Found: C, 45.15; H, 5.08; N, 5.04%. FT-IR (KBr, cm^{-1}): 1607 ($\nu_{C=N}$); 2938 (ν_{C-H}); 3363 (ν_{O-H}). UV-vis, λ_{max} (nm), [ε_{max} (L mol^{-1} cm^{-1})] (CH_3CN), 230 (4.9×10^4), 288 (2.2×10^4), 393 (1.03×10^4), 570 (4.6×10^3). Magnetic moment = 5.03 B. M. HRMS (ESI, positive ion mode, acetonitrile) *m*/*z*: 423.0227 (cald. 423.37) for $[Mn(L^2)]^+$.

Synthesis of $[MnL^3(DMSO)(H_2O)]ClO_4$ (3). 5-Chlorosalicyldehyde (0.315 g, ∼2 mmol) and 2,2-dimethylpropane-1,3-diamine (0.13 mL, ∼1 mmol) were refluxed in 10 mL of methanol for around 4 hours at a 2 : 1 molar ratio. The solution mixture was then cooled to room temperature. A methanol/water (4 : 1) solution (5 mL) of manganese(II) perchlorate hexahydrate (0.362 g, ∼1 mmol) was added to it with continuous stirring. The colour of the solution changes from yellow to dark brown. A few drops of DMSO were added to the reaction mixture. The reaction mixture was then kept undisturbed for slow evaporation in an open atmosphere. Deep brown block-shaped single crystals of **3**, suitable for X-ray diffraction, were obtained after 10–11 days. It was re-crystallized from DMSO.

Complex **3**: yield: 434 mg (∼69%). Calc. for $C_{21}H_{26}Cl_3MnN_2O_8S$ (FW 627.79): C, 40.18; H, 4.17; N, 4.46%. Found: C, 40.24; H, 4.32; N, 4.53%. FT-IR (KBr, cm^{-1}): 1605–1632 ($\nu_{C=N}$); 2949 (ν_{C-H}); 3370 (ν_{O-H}). UV-vis, λ_{max} (nm), [ε_{max} (L mol^{-1} cm^{-1})] (CH_3CN), 224 (2.86×10^4), 277 (1.41×10^4), 388 (5.2×10^3), 520 (9.6×10^2). Magnetic moment = 5.01 B. M. HRMS (ESI, positive ion mode, acetonitrile) *m*/*z*: 430.9119 (cald. 432.21) for $[Mn(L^3)]^+$.

Synthesis of $[MnL^4(DMSO)(H_2O)]ClO_4$ (4). Complex **4** was synthesized in a similar method where 3-ethoxysalicyldehyde (0.332 g, ∼2 mmol) and 2-hydroxypropane-1,3-diamine (0.10 mL, ∼1 mmol) were used instead of 5-chlorosalicyldehyde and 2,2-dimethylpropane-1,3-diamine. It was re-crystallized from DMSO.

Complex **4**: yield: 405 mg (∼64%). Calc. for $C_{23}H_{30}ClMnN_2O_{11}S$ (FW 632.95): C, 43.64; H, 4.78; N, 4.43%. Found: C, 43.67; H, 4.79; N, 4.44%. FT-IR (KBr, cm^{-1}): 1603 ($\nu_{C=N}$); 2936 (ν_{C-H}); 3403 (ν_{O-H}). UV-vis, λ_{max} (nm), [ε_{max} (L mol^{-1} cm^{-1})] (CH_3CN), 228 (3.93×10^4), 287 (1.7×10^4), 391 (6.5×10^3), 567 (3.9×10^3). Magnetic moment = 5.03 B. M. HRMS (ESI, positive ion mode, acetonitrile) *m*/*z*: 439.0023 (cald. 437.35) for $[Mn(L^4)]^+$.

Physical measurements. A PerkinElmer 240C analyzer was used to perform elemental analyses for carbon, hydrogen, and nitrogen. In addition, IR spectra within the range of 4000–500 cm^{-1} were recorded using a PerkinElmer RX-1 FTIR spectrophotometer with KBr. Electronic spectra were also recorded using a SHIMADZU UV-vis-spectrofluorometer (UV1900i). The magnetic susceptibility measurement was performed with an EG and PAR vibrating sample magnetometer, model 155 at room temperature (300 K) in a 5000 G magnetic field, and diamagnetic corrections were performed using Pascal's constants. The Waters Xevo G2 Q-TOF was used to record the electrospray ionization mass spectra.

X-Ray crystallography

Suitable single crystals of all complexes were collected and mounted on glass fibers. A 'Bruker D8 QUEST area detector', equipped with graphite-monochromated Mo-K_α radiation (λ = 0.71073 Å), was used to measure the diffraction intensities of the complexes. The molecular structures were solved by direct methods and refined by full-matrix least squares on F^2, using the SHELX-16/3 program.[31] Anisotropic thermal parameters were used for the refinement of non-hydrogen atoms. Hydrogen

Table 1 Selected bond lengths (Å) and bond angles (°) of complexes **1–4**[a]

Complex	1	2	3	4
Mn(1)–O(1)	1.881(2)	1.898(2)	1.865(4)	—
Mn(1)–O(2)	1.903(2)	1.894(2)	1.892(4)	1.890(2)
Mn(1)–N(1)	2.026(3)	2.023(3)	2.013(5)	2.040(3)
Mn(1)–N(2)	2.030(3)	2.036(3)	1.997(5)	—
Mn(1)–O(3)	2.206(2)	2.233(3)	2.193(5)	2.251(3)
Mn(1)–O(4)	2.221(2)	2.225(3)	2.326(5)	2.248(4)
O(1)–Mn(1)–O(2)	85.04(10)	87.37(10)	88.9(2)	—–
O(1)–Mn(1)–O(3)	89.64(11)	90.99(10)	98.1(2)	—–
O(1)–Mn(1)–O(4)	94.23(11)	92.37(11)	89.7(2)	—–
O(1)–Mn(1)–N(1)	90.43(11)	89.19(12)	91.3(2)	—
O(1)–Mn(1)–N(2)	174.44(12)	177.14(11)	175.6(2)	—
O(2)–Mn(1)–O(3)	92.86(11)	91.91(10)	90.1(2)	92.41(9)
O(2)–Mn(1)–O(4)	91.79(11)	94.33(11)	94.5(2)	91.40(10)
O(2)–Mn(1)–N(1)	175.45(10)	176.49(15)	178.6(2)	90.45(10)
O(2)–Mn(1)–N(2)	90.53(11)	89.82(12)	90.6(2)	—
O(3)–Mn(1)–O(4)	174.20(10)	173.04(10)	171.0(2)	174.81(11)
O(3)–Mn(1)–N(1)	87.52(12)	88.82(11)	88.5(2)	87.63(9)
O(3)–Mn(1)–N(2)	87.21(11)	88.59(11)	86.2(2)	—
O(4)–Mn(1)–N(1)	88.13(11)	85.13(11)	87.0(2)	88.82(10)
O(4)–Mn(1)–N(2)	89.27(11)	88.35(12)	86.0(2)	—
N(1)–Mn(1)–N(2)	94.01(11)	93.63(13)	89.3(2)	—
O(2)–Mn(1)–O(2)[a]	—	—	—	85.44(12)
O(2)–Mn(1)–N(1)[a]	—	—	—	175.89(9)
N(1)–Mn(1)–N(1)[a]	—	—	—	93.66(14)

[a] Symmetry transformation, [a] = x, 1 − y, z.

atoms attached to oxygen atoms were located by different Fourier maps and were refined with distance constraints where possible else kept at fixed positions. All other hydrogen atoms were placed in their geometrically idealized positions and constrained to ride on their parent atoms. In **4**, disorder was found in the DMSO and the CH–OH moiety of the ligand. Multi-scan empirical absorption corrections were applied to the data using the program SADABS.[32] The details of crystallographic data and refinements of all complexes are listed in Table S1.† Important bond lengths and bond angles are given in Table 1.

Computational details

The calculations reported herein were performed using the Turbomole 7.2 program.[33] The crystallographic coordinates were used for the calculations of the supramolecular assemblies. We used the crystallographic coordinates for the assemblies because we are interested in evaluating the interactions as they stand in the solid state. The level of theory used for the calculations was RI-BP86-D3/def2-TZVP.[34–38] The MEP surface plots were generated using the wavefunction obtained at the same level of theory and the 0.001 a.u. isosurface to simulate the van der Waals envelope. The topological analysis of the electron density was carried out according to the quantum theory of atoms in molecules (QTAIM) method proposed by Bader[39] and the reduced density gradient (RDG) isosurfaces (NCIplot)[40] and represented using the VMD program.[41] They were computed using the MultiWFN program[42] at the PB86-D3/def2-TZVP level of theory. The NBO analysis[43] was performed using the same level of theory and the NBO 7.0 program.[44]

Hirshfeld surface analysis

The structure input files in CIF format was used to calculate the Hirshfeld surfaces[45–47] and the associated 2D-fingerprint plots[48–50] using Crystal Explorer software.[51] The Hirshfeld surface is a crucial and useful tool for studying intermolecular interactions while preserving a whole-molecule perspective. The proximity of intermolecular contacts in a molecule is well defined by parameters d_e and d_i, where d_e refers to the distances

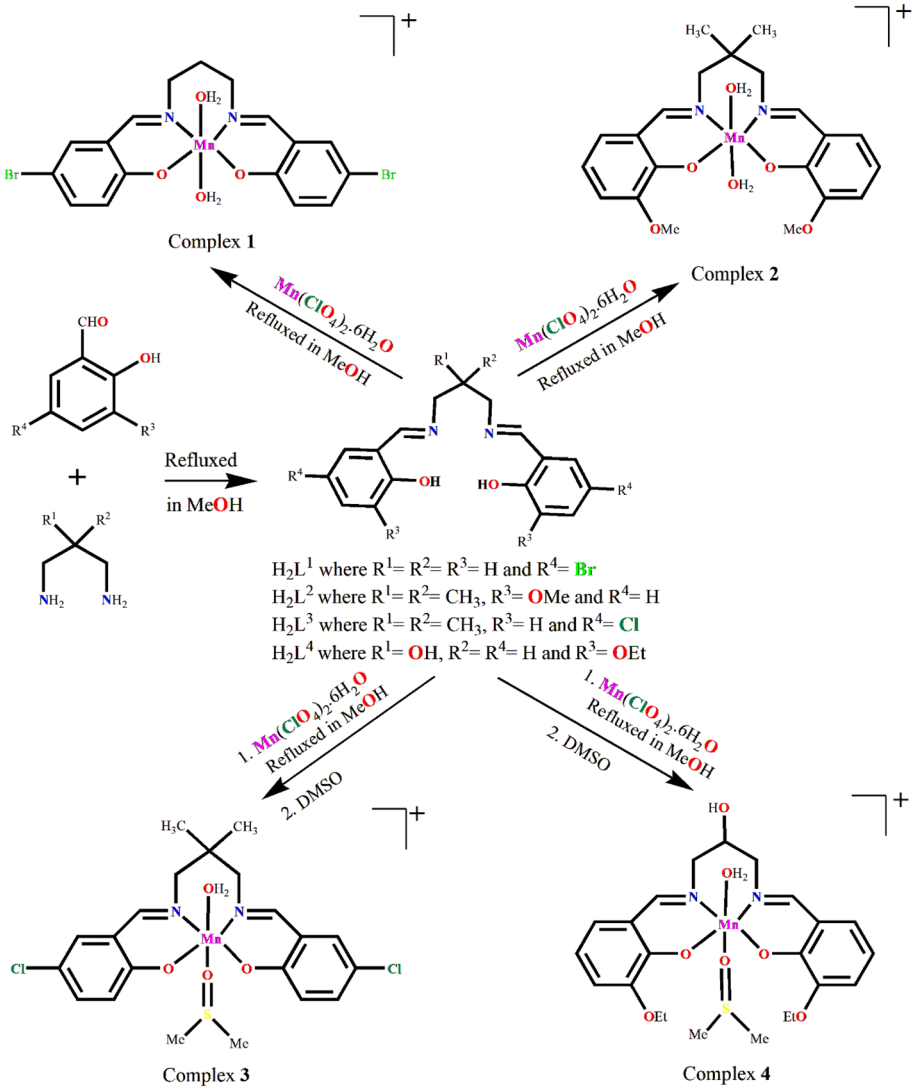

Scheme 3 Synthetic route to complexes **1**–**4**. Counter perchlorate anions and lattice solvent molecules, if any, have been omitted for clarity.

Table 2 The deviations of all the four coordinating atoms (Å) in the basal plane from the mean plane passing through them and that of manganese(III) from the same plane

Complex	N(1)	N(2)	O(1)	O(2)	Mn(III)
1	0.029(2)	−0.028(2)	−0.033(2)	0.033(2)	−0.026(2)
2	0.009(2)	−0.009(2)	−0.010(2)	0.010(2)	0.001(2)
3	0.046(2)	−0.047(2)	−0.050(3)	0.050(3)	0.024(2)
4	0.000	—	0.000	—	0.051(2)

to the nearest atoms outside, and d_i refers to distances to the nearest atoms inside respectively. Another parameter, d_{norm}, has been introduced to account for the relative sizes of atoms. A distinctive red-white-blue colour scheme has been used to display intermolecular contacts. The red spots on the Hirshfeld map indicate shorter contacts, white spots denote the contacts around the van der Waals separation and blue spots are for larger contacts. The interactions in the crystal are succinctly summarised by 2D-fingerprint displays.

Results and discussion

Synthesis

The Schiff bases (H_2L^1–H_2L^4) were prepared by refluxing the appropriate diamine and salicylaldehyde derivatives in 1 : 2 molar ratio in methanol following the literature method.[52–56] These Schiff bases were not isolated and purified, but the methanol solution of the Schiff bases were used *in situ* for the synthesis of manganese(III) complexes, $[MnL^1(H_2O)_2]ClO_4 \cdot H_2O$ (**1**), $[MnL^2(H_2O)_2]ClO_4$ (**2**), $[MnL^3(DMSO)(H_2O)]ClO_4$ (**3**), $[MnL^4(DMSO)(H_2O)]ClO_4$ (**4**) by adding manganese(II) perchlorate hexahydrate with constant stirring. The formation of the complexes is shown in Scheme 3. It is to be mentioned here that all the ligands have already been well characterized and used by different research groups for the synthesis of different transition and non-transition metal complexes for many years.[57–66]

In the present case, mononuclear octahedral complexes containing the tetradentate Schiff base ligands (dianions of H_2L^1, H_2L^2, H_2L^3, and H_2L^4 respectively) are formed, with one/

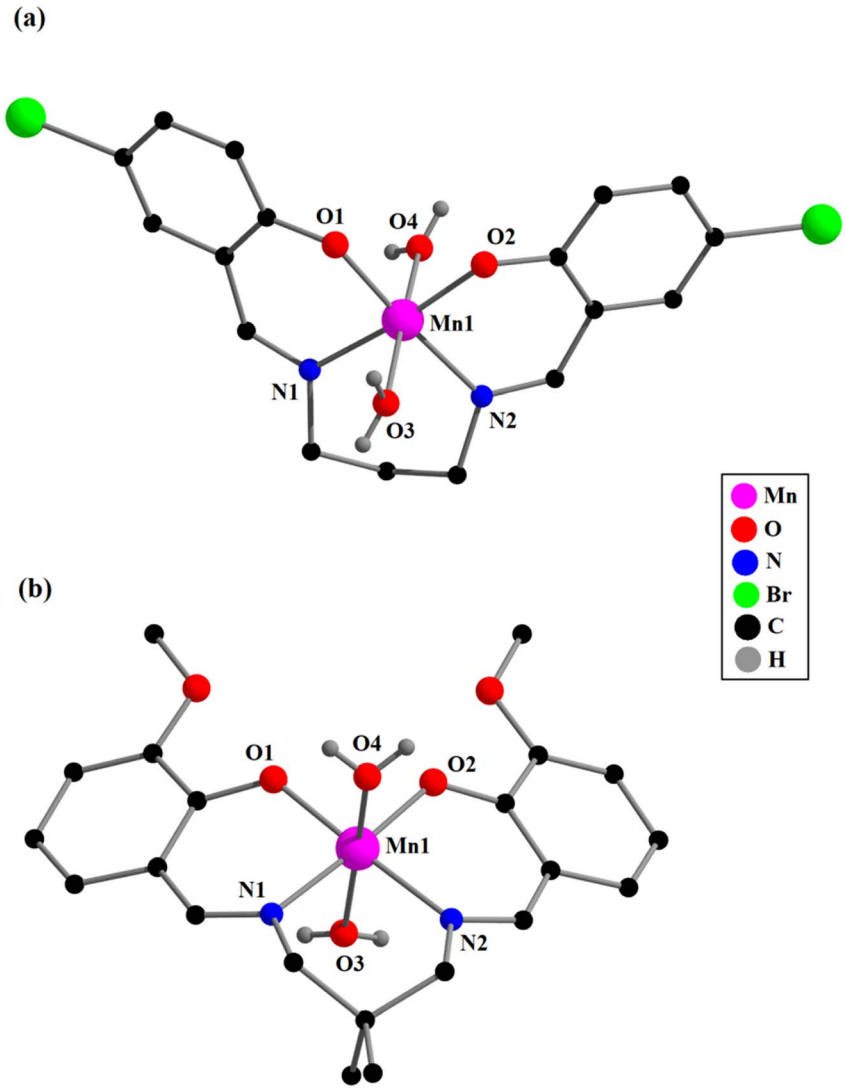

Fig. 1 Perspective views of complexes **1** (a) and **2** (b) with the selective atom numbering scheme. All the hydrogen atoms (except those of coordinating water molecules), the non-coordinated perchlorate ions, and a lattice water molecule have been omitted for clarity.

two coordinating water molecule(s). In each case manganese(II) is converted to manganese(III) species by aerial oxidation, as has also been observed previously.[67–69] Thus, the efforts to prepare complexes in N_2 or Ar atmosphere were not successful. X-Ray-quality single crystals of complexes **3** and **4** were grown in DMSO medium. We have tried to obtain single crystals of **3** and **4** from other solvents also, but the efforts were unsuccessful. X-Ray diffraction data shows that one DMSO molecule is as co-ligand in the coordination sphere of manganese(III) in each of complexes **3** and **4** (*vide infra*) and this explains the necessity of using DMSO in their synthesis.

It is to be mentioned here that complexes with coordinated water molecules may open up the possibilities of preparing several water-bridged dimeric complexes. To understand the mechanism of ligand replacement reactions, complexes with coordinated water molecules are important. In each complex, the hydrogen atoms of the water molecules are involved in H-bonding.

Description of structures

Description of structures of complexes 1–4. The X-ray structure determinations reveal that each complex consists of mononuclear cation of type, $[MnL(X)(Y)]^+$ along with a non-coordinated perchlorate counter anion; X = Y=H_2O for complexes $[MnL^1(H_2O)_2]ClO_4 \cdot H_2O$ (**1**) and $[MnL^2(H_2O)_2]ClO_4$ (**2**), whereas X = H_2O and Y = DMSO for complexes $[MnL^3(DMSO)(H_2O)]ClO_4$ (**3**) and $[MnL^4(DMSO)(H_2O)]ClO_4$ (**4**); L = L^1 (in **1**), L^2 (in **2**), L^3 (in **3**), and L^4 (in **4**). A lattice water molecule is also present in the asymmetric unit of complex **1**. Complex **1** crystallizes in the orthorhombic space group $P2_12_12_1$. Complex **2** crystallizes in the monoclinic space group $C2/c$. Single-crystal X-ray analysis reveals that complex **3** crystallizes in the orthorhombic space group $P\bar{1}$. Single crystal X-ray diffraction analysis reveals that complex **4** crystallizes in the monoclinic space group $C2/m$ and has mirror symmetry.

Each mononuclear complex contains a manganese(III) center with six-coordination pseudo-octahedral geometry. In each

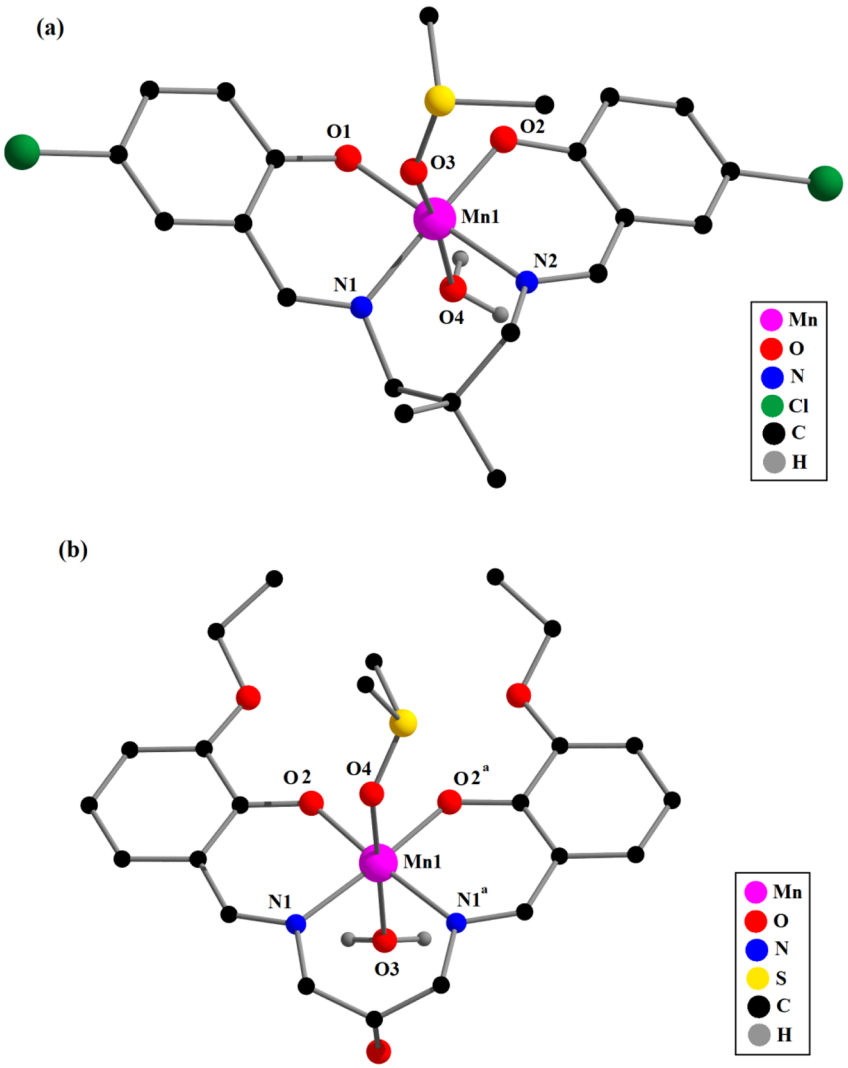

Fig. 2 Perspective views of complexes **3** (a) and **4** (b) with the selective atom numbering schemes. All the hydrogen atoms (except hydrogen-atoms of coordinating water molecules) and a non-coordinated perchlorate ion are omitted for clarity. In **4**, which has mirror symmetry, only the major component of the disordered CH–OH group and the DMSO ligand is shown. Symmetry transformation, $^a = x, 1 - y, z$.

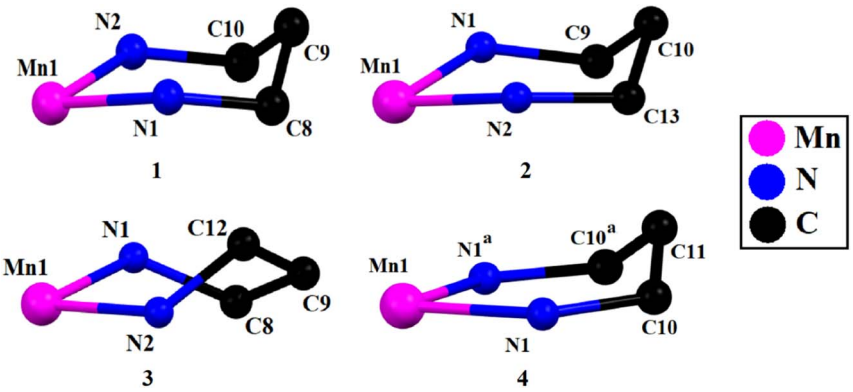

Fig. 3 Half-chair conformations of six-membered chelate rings in complexes **1** and **2**. Twist-boat conformation of six-membered chelation ring of complex **3**. Envelope like conformation of six-membered chelation ring of complex **4**. Symmetry transformation, $^{a} = x, 1 - y, z$.

Table 3 Puckering analysis for saturated six-membered chelate rings[a]

		Puckering amplitude, q (Å)	Torsion angle, θ (°)	Phase angle, ϕ (°)	Conformation
1	Mn(1)–N(1)–C(8)–C(9)–C(10)–N(2)	0.526(4)	32.4(3)	173.8(7)	Approximate half-chair
2	Mn(1)–N(1)–C(9)–C(10)–C(13)–N(2)	0.540(5)	146.7(4)	351.2(8)	Approximate half-chair
3	Mn(1)–N(1)–C(8)–C(9)–C(12)–N(2)	0.745(7)	89.1(5)	261.9(5)	Twist boat
4	Mn(1)–N(1)–C(10)–C(11)–C(10)^{a}–N(1)^{a}	0.498(7)	115.5(6)	360.0(6)	Approximate envelope

[a] Symmetry transformation, $^{a} = x, 1 - y, z$.

complex, two imine nitrogen atoms {N(1) and N(2) for complexes **1–3**; and N(1), N(1)^{a} for complex **4**}, and two phenolate oxygen atoms, {O(1) and O(2) for complexes **1–3**; and O(2), O(2)^{a} for complex **4**}, of the deprotonated di-Schiff base (L^{2-}) constitute the equatorial plane {symmetry transformation, $^{a} = x, 1 - y, z$}. Two oxygen atoms {O(3) and O(4)} from two coordinated water molecules (in **1** and **2**) or one from water and another from DMSO (in **3** and **4**), are attached to the manganese(II) centers in axial sites. Manganese(III)–oxygen and manganese(III)–nitrogen distances fall within the range observed for structurally characterized manganese(III) complexes.[1–17] The axial manganese(III)–oxygen distances are much longer compared to the equatorial manganese(III)–oxygen and manganese(III)–nitrogen distances (Table 1), as were also observed in similar complexes.[1–17] The elongation of axial bonds indicates clear evidence of Jahn–Teller distortion, as expected for high-spin manganese(III) with d^4 ($t_{2g}^3 e_g^1$) electronic configuration. The basal bond angles are all close to 90° (Table 1). The donor atoms, {O(1), O(2), N(1), N(2) in complexes **1–3**; and O(2), O(2)^{a}, N(1), N(1)^{a} in **4**} in the equatorial plane are approximately co-planar with no atoms deviating from the plane by more than 0.050 Å in any complex. The deviations of all the coordinating atoms in the basal plane from the mean plane passing through them and that of manganese(III) from the same plane are gathered in Table 2. The perspective views of complexes along with the selected atom numbering scheme is shown in Fig. 1 and 2.

The saturated six-membered chelate rings [Mn(1)–N(1)–C(8)–C(9)–C(10)–N(2) in **1**, Mn(1)–N(1)–C(9)–C(10)–C(13)–N(2) in **2**, Mn(1)–N(1)–C(8)–C(9)–C(12)–N(2) in **3**, and Mn(1)–N(1)–C(10)–C(11)–C(10)^{a}–N(1)^{a} in **4**] have different conformations, as confirmed by puckering analysis.[70–72] The conformation of the rings are shown in Fig. 3 while their puckering parameters are given in Table 3.

DFT study on supramolecular interaction

The DFT study is focused on two main aspects of the solid-state structures of complexes **1–4**. One is the formation of halogen (HaB) and chalcogen bonding (ChB) interactions in complexes **1** and **3** where the electron donor is the perchlorate anion and the acceptor either bromine or chlorine atoms for the HaBs and the sulfur atom of the coordinated DMSO for the ChB. The other one is the analysis of the formation of recurrent motifs in the solid state of complexes **1**, **2** and **4**. They consist of supramolecular dimers where the hydrogen atoms of the coordinated water molecules interact with the electron rich cavity formed by the phenolic and alkyloxy oxygen atoms of the Schiff-base ligand. Dimensions of the hydrogen bonds in the structures are given in Table 4.

First, we have analyzed the MEP surfaces of complexes **1**, **2** and **4** in order to investigate the relative basicity of the oxoanionic cavity. It should be emphasized that the manganese(III) complexes are positive, and consequently in these calculations we have included the counterion to keep the global system

Table 4 Hydrogen bonds in the complexes

Complex	Atoms involved (D–H···A)	Distance D–H (Å)	Distance H···A (Å)	Distance D···A (Å)	Angle ∠D–H···A (°)	Symmetry
1	O4–H3W···O1	0.82	2.30	3.079(4)	158.3(2)	$x + 1/2, 3/2 - y, 1 - z$
	O4–H3W···O2	0.82	2.44	2.982(3)	124.6(2)	$x + 1/2, 3/2 - y, 1 - z$
	O3–H1W···O1	0.82(3)	2.64(6)	3.108(4)	117(5)	$x - 1/2, 3/2 - y, 1 - z$
	O3–H1W···O2	0.82(3)	2.06(2)	2.879(3)	175(6)	$x - 1/2, 3/2 - y, 1 - z$
	O3–H2W···O10	0.85(2)	1.99(3)	2.799(4)	159(6)	$-1 + x, y, z$
	O4–H4W···O10	0.85(2)	1.95(3)	2.794(4)	173(6)	
	O10–H10W···O6	0.83(2)	1.96(2)	2.789(4)	173(6)	$2 - x, y - 1/2, 3/2 - z$
	O10–H11W···O8	0.82(2)	2.09(3)	2.894(6)	169(7)	
	C5–H5···Br2	0.93	3.03	3.949(4)	170.5	$x, -1 + y, z$
	C11–H11···O8	0.93	2.64	3.273(5)	125.8	$-1 + x, y, z$
	C13–H13···O6	0.93	2.61	3.428(5)	146.5	$-1 + x, y, z$
2	O4–H3W···O5	0.85(2)	1.93(3)	2.761(4)	164(10)	$-x + 3/2, y + 1/2, -z + 3/2$
	O4–H4W···O6	0.85(2)	2.03(4)	2.840(4)	160(11)	$-x + 3/2, y + 1/2, -z + 3/2$
	O3–H2W···O2	0.85(2)	2.05(5)	2.811(4)	149(9)	$-x + 3/2, y - 1/2, -z + 3/2$
	O3–H2W···O6	0.85(2)	2.68(9)	3.107(4)	113(8)	$-x + 3/2, y - 1/2, -z + 3/2$
	O3–H1W···O1	0.85(2)	2.10(6)	2.778(3)	137(7)	$-x + 3/2, y - 1/2, -z + 3/2$
	O3–H1W···O5	0.85(2)	2.41(7)	3.092(4)	138(8)	$-x + 3/2, y - 1/2, -z + 3/2$
	C8–H8···O8	0.93	2.59	3.433(8)	151.4	
3	O4–H1W···O2	0.85(2)	1.92(3)	2.762(6)	171(12)	$2 - x, 1 - y, 1 - z$
	O4–H2W···O5	0.86(2)	2.23(6)	3.044(9)	158(13)	
	C5–H5···O8	0.93	2.60	3.227(11)	124.8	
	C7–H7···O8	0.93	2.57	3.365(11)	144.1	$1 - x, 2 - y, 1 - z$
	C8–H8B···O3	0.97	2.56	3.148(9)	119.3	
	C12–H12B···O4	0.97	2.56	3.199(8)	123.0	
	C13–H13···O7	0.93	2.40	3.188(11)	141.8	$1 - x, 1 - y, 1 - z$
	C20–H20C···O1	0.96	2.57	3.399(12)	144.7	
	C21–H21B···Cl2	0.96	2.95	3.886(10)	165.2	$x, 1 + y, z$
	C21–H21B···O6	0.96	2.791	3.44(2)	125.6	$x, y, 1 + z$
	C20–H20B···O6	0.96	2.811	3.46(2)	125.2	$x, y, 1 + z$
4	O3–H3···O1	0.84(2)	2.05(4)	2.855(3)	159(10)	$1 - x, 1 - y, 1 - z$
	O3–H3···O2	0.84(2)	2.44(7)	3.049(3)	130(7)	$1 - x, 1 - y, 1 - z$
	O5A–H5A···O4	0.850(5)	2.000(5)	2.835(6)	167(4)	
	O5B–H5B···O3	0.861(5)	2.014(3)	2.874(5)	176.7(7)	
	C1–H1B···O5B	0.96	2.42	3.371(9)	169.9	$1 - x, 1 - y, 1 - z$
	C9–H9···O12	0.93	2.53	3.441(7)	166.6	$1/2 - x, 3/2 - y, -z$
	C11B–H11B···O5B	0.98	1.78	2.568(16)	135.3	$1 - x, 1 - y, -z$
	C12–H12B···O2	0.96	2.49	3.345(6)	147.9	$x, 1 - y, z$

neutral. The MEP surfaces are plotted in Fig. 4, evidencing that in all cases the global MEP minimum is located at the perchlorate anion (ranging −60 to −69 kcal mol^{-1}) and the maximum at the coordinated water protons (ranging +65 to +75 kcal mol^{-1}). In all cases, the MEP is negative at the region under the influence of both phenolate oxygen atoms, in spite of

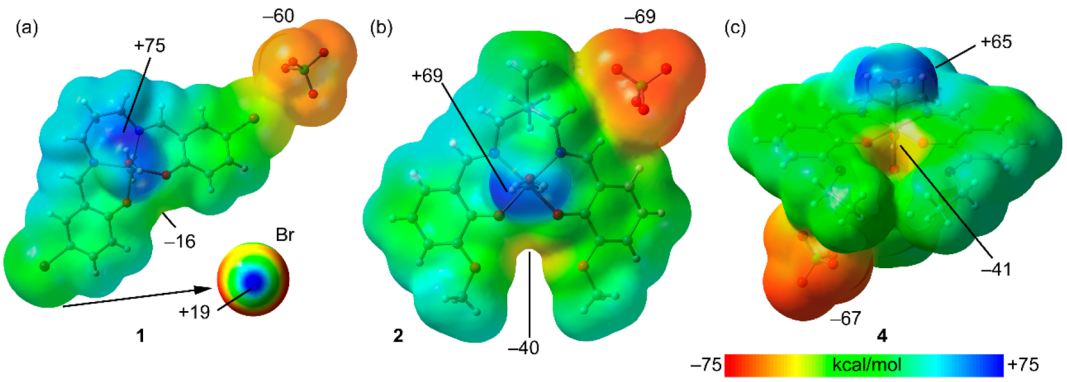

Fig. 4 MEP surfaces of complexes **1** (a), **2** (b) and **4** (c) at the RI-BP86-D3/def2-TZVP level of theory. The values at selected points of the surfaces are given in kcal mol^{-1}. Isovalue 0.001 a.u.

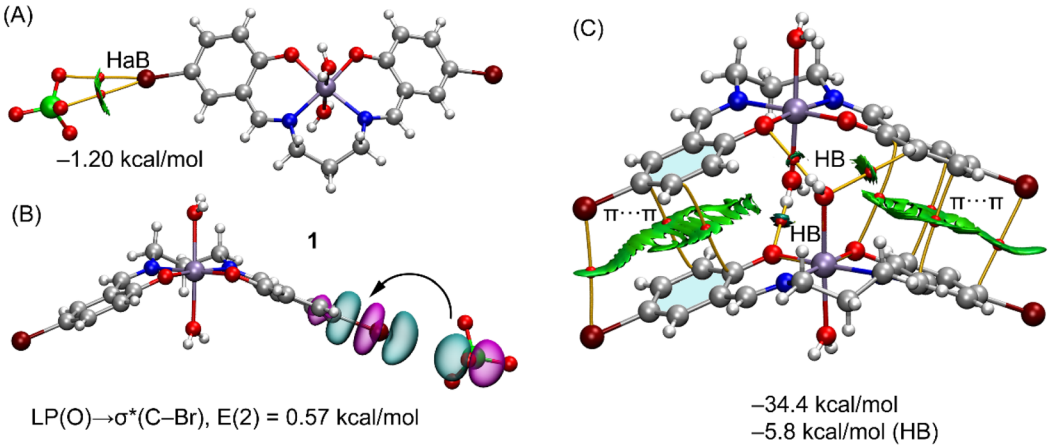

Fig. 5 (A) QTAIM (bond CPS in red and paths as orange lines) and NICPlot (see computational method for details) characterization of the HaB interaction. (B) NBOs involved in the LP(O) → σ*(C–Br) interaction. (C) QTAIM/NCIplot analysis of the self-assembled dimer in **1**. Only intermolecular interactions are represented. The counterions are omitted in the representation of (c), though they were taken into consideration for the calculation of the interaction energies. The HB contribution has been estimated using the V_r values at the bond CPs that characterize the HBs.

the global positive charge of the manganese(III) complex. The presence of the extra oxygen atoms from the methoxy (**2**) and ethoxy (**4**) groups significantly increases the ability of the O_4-cavity to interact with electron poor atoms. Finally, the MEP surface analysis of complex **1** also revels the presence of a σ-hole at the bromine atoms (+19 kcal mol^{-1}), as highlighted in Fig. 4a (bottom-right) using a reduced MEP scale (+19 to 0 kcal mol^{-1}).

Fig. 5a shows the QTAIM/NCIplot analysis of the interaction of the perchlorate with the manganese(III) complex, disclosing the formation of a bifurcated HaB, that is characterized by two bond critical points (CPs, red spheres) and bond paths (orange lines) connecting two oxygen atoms of the anion to the bromine atom. The interaction is further characterized by a green RDG (reduced density gradient) isosurface (green color is used herein to indicate weak and attractive NCI) that is located between the bromine-atom of both oxygen atoms of the anion. In order to estimate the strength of the bifurcated HaB free from the pure coulombic attraction between the counterions, we have used the method proposed by Bartashevich and Tirelson[73] that is based on the value of the potential energy density V_r at the bond CP. As a result, the HaB estimation is −1.20 kcal mol^{-1}, in line with the green color of the RDG isosurface and revealing its modest strength. This HaB has been also studied from an orbital point of view using the natural bond orbital (NBO) analysis and focusing on the second order perturbation analysis, since it is very convenient to analyze orbital donor–

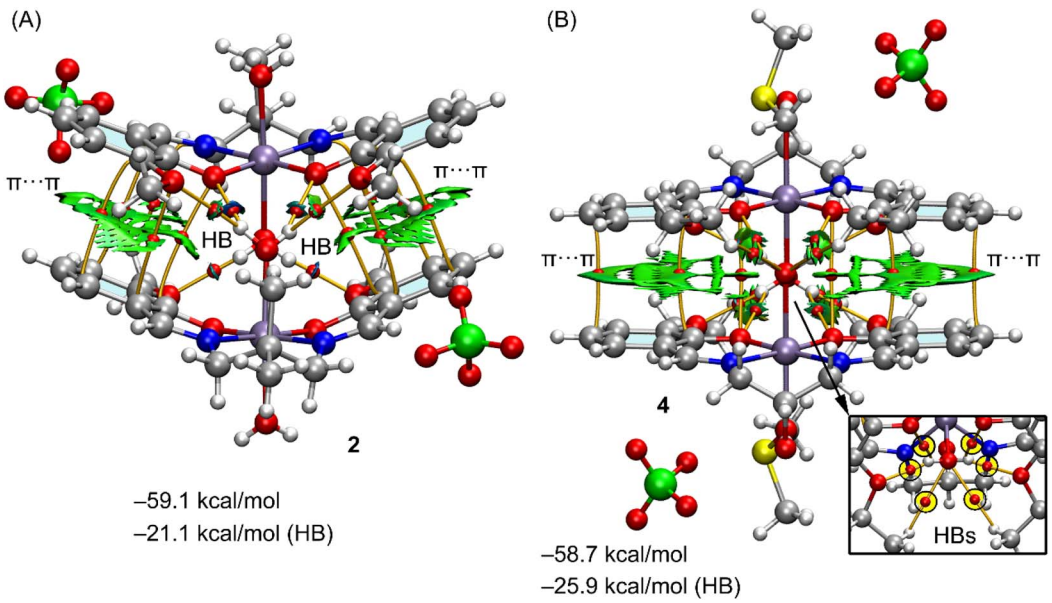

Fig. 6 (A) QTAIM (bond CPS in red and paths as orange lines) and NICPlot (see computational method for details) analysis of the self-assembled dimers in **2** (A) and **4** (B). Only intermolecular interactions are represented. The HB contributions have been estimated using the V_r values at the bond CPs that characterize the HBs.

acceptor interactions. Interestingly, the NBO method discloses an electron transfer from the lone pairs at the oxygen-atoms of the perchlorate to the antibonding σ*(C–Br) orbital with a concomitant stabilization energy of 0.57 kcal mol^{-1}, and confirming the σ-hole nature of the interaction. The NBOs involved in one of both LP(O) → σ*(C–Br) interactions is shown in Fig. 5B.

In the crystal the packing of complex **1** shows a polymer formed by successive hydrogen bonds involving the coordinated water molecules and the phenolate oxygen atoms formed along the crystallographic *a* axis (Table 4). A model has been abstracted, shown in Fig. 5C of two adjacent molecules in these polymers in which the coordinated water molecule, O(3), of one manganese(III) complex forms donor hydrogen bonds to the acceptor phenolate oxygen atoms of the adjacent molecule {symmetry $-1/2 + x$, $3/2 - y$, $1 - z$}. The second axial water molecule, O(4), forms similar donor hydrogen bonds in this dimer. Also involved is the water molecule, O(10), which acts as an acceptor to the coordinated water molecules and as a donor to two perchlorate oxygen atoms. Using the dimeric model, three H-bonds are established, each one characterized by the corresponding bond CP, bond path and green-blue isosurface. The total contribution of the HBs using the V_r energy predictor is −5.8 kcal mol^{-1}. The formation of the dimer is further supported by π-stacking interactions, characterized by several bond CPs and bond paths interconnecting the aromatic rings with a distance of 3.92 Å between centroids. Moreover, the interactions are further characterized by extended green isosurfaces that embrace the whole aromatic surfaces and the C–Br bonds. The total interaction energy is very large (−34.4 kcal mol^{-1}) due to the electrostatic contribution (ion pair attraction), between the perchlorate anions (not shown in Fig. 5C for clarity) and the cationic manganese(III) complexes.

Both complexes **2** and **4** also form polymers but for simplicity only dimers are considered in the calculations and these are shown in Fig. 6, including their QTAIM/NCI plot analysis. Both dimers show extended RDG isosurfaces between the aromatic ring, disclosing the existence of π-stacking interactions. These are also evidenced by several bond CPs and bond path interconnecting the rings. Both dimers exhibit very large dimerization energies, due to the electrostatic attraction between the counterions. In complex **2**, one of the water molecules, O(4), establishes four H-bonds with the four oxygen-atoms of the electron rich O_4-cavity from the adjacent molecule {symmetry $-x + 3/2$, $y - 1/2$, $-z + 3/2$}. In this dimer, the second water molecule, O(3), only forms two hydrogen bonds to the two uncoordinated methoxy atoms, O(5) and O(6). Presumably as a consequence of the formation of so many hydrogen bonds involving the coordinated water molecules, listed in Table 4, there are no such bonds involving the perchlorate oxygen atoms. The other water molecule involved in the formation of this dimer establishes only two H-bonds with the methoxy groups. The overall contribution of the six H-bonds in the dimer of **2** is −21.1 kcal mol^{-1}, confirming the importance of the OH···O interactions and supporting the relevance of this motif in the solid state.

In complex **4**, the metal has mirror symmetry, and the coordinated water molecule, O(3), establishes four donor H-bonds (see Fig. 6B, bottom-right), to O(1)*2 and O(2)*2 in the electron rich O_4-cavity of a neighboring $(1 - x, y, 1 - z)$ symmetry related molecule to form the dimer. An additional H-bond is found from the disordered CH–OH group in the ligand. There are two alternative positions for the oxygen, named O(5A) and O(5B) with respective populations of 0.35(2), 0.65(2) and the coordinated water molecule, O(3) forms an acceptor H-bond to O(5B) while the O(4), from DMSO, forms an acceptor H-bond to O(4B). All H-bond dimensions are given in Table 4.

Consequently the contribution of the H-bonds (−25.9 kcal mol^{-1}) is larger in **4** than in the dimer of **2** (−21.1 kcal mol^{-1}). The large contribution of the H-bonds and the formation of the four H-bonds between the water molecule and the electron rich cavity and hydrogen-atoms of the ethoxy groups reveals a strong complementarity between the water molecules and the cavity and explains the formation of such binding motif in the solid state. It is also worth mentioning such motifs are governed by the cooperation of the H-bonds and π-stacking interactions, even in the presence of stronger but non-directional electrostatic forces. It is interesting to note that as in **2**, which also contains alkoxy groups, there are no hydrogen bonds involving the perchlorate anion.

Finally, in complex **3**, the coordinated water molecule forms two donor hydrogen bonds, one to perchlorate oxygen atom, O(5) and the other to a ligand oxygen, O(2) of a neighboring symmetry related $(2 - x, 1 - y, 1 - z)$ complex molecule. However the most notable interactions are observed where the perchlorate anion bridges two manganese(III) complexes (symmetry transformations, x, y, z and $x, 1 + y, z$) by means of the formation of two concurrent σ-holes (HaB and ChB). In particular, one oxygen-atom, O(6), in the perchlorate is located opposite to the S=O bond of the coordinated DMSO molecule and also opposite to the C(16)–Cl(2) bond, thus establishing both ChB and HaB interactions. Both contacts have been confirmed by QTAIM analysis, showing bond CPs and bond paths connecting one oxygen-atom of the anion to the chlorine and sulfur atoms of the Schiff-base and DMSO ligands, respectively, as detailed in Fig. 7A. Two CH bonds (C20–H20B and C21–H21B) of the DMSO are also connected with the oxygen atom, O(6), thus forming two additional CH···O interactions. All interactions are also revealed by the NCIplot analysis and characterized by green colored RDG isosurfaces. Fig. 7B shows the NBOs involved in the interactions, showing two contributions: LP(O) → σ*(C–Cl) and LP(O) → σ*(S–O), thus confirming the σ-hole nature of both interactions. Moreover, the second order stabilization energies disclose that the ChB is slightly stronger ($E(2)$ = 1.75 kcal mol^{-1}) than the HaB ($E(2)$ = 1.59 kcal mol^{-1}).

Hirshfeld surface analysis

Hirshfeld surface analysis of complexes **1–4** was performed to identify and emphasize the significant intermolecular interactions that exist in their solid-state structures. The surfaces were kept transparent to visualize the molecular moiety clearly.

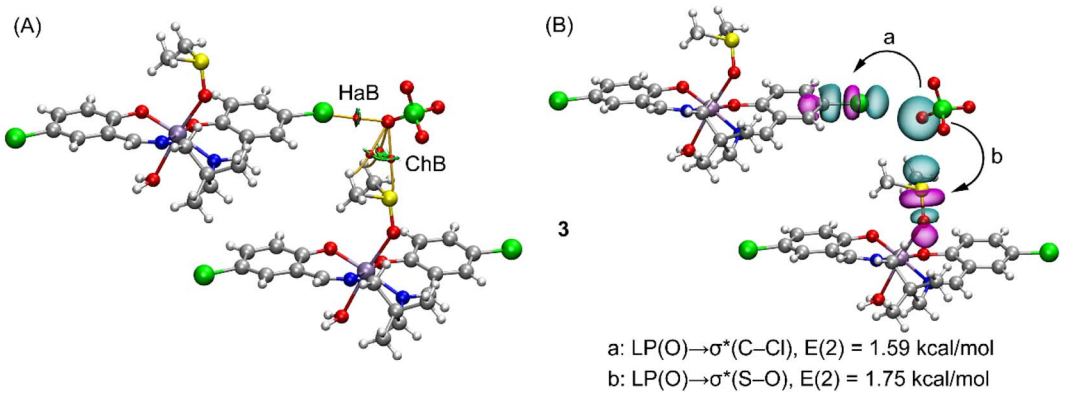

Fig. 7 (A) QTAIM (bond CPs in red and paths as orange lines) and NICPlot (see computational method for details) characterization of the HaB and ChB interactions in complex **3**. (B) NBOs involved in the LP(O) → σ*(C–Cl) and LP(O) → σ*(S–O) interactions.

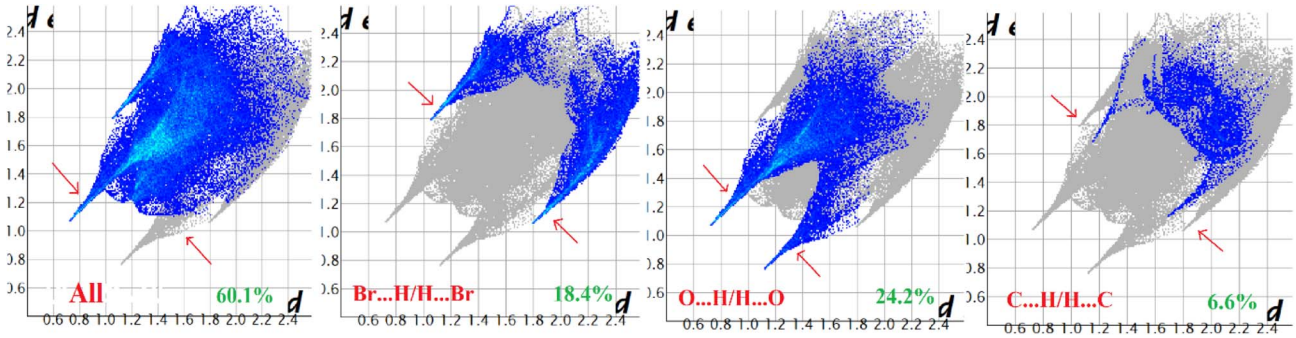

Fig. 8 Fingerprint plot of complex **1**: full and resolved into Br···H/H···Br, O···H/H···O, and C···H/H···C contacts contributed to the total Hirshfeld surface area.

Fig. S1 (ESI†) illustrates the mapping of the Hirshfeld surface for each complex, utilizing d_{norm} in the range of −0.1 Å to 1.5 Å, as well as shape index and curvedness. The Hirshfeld surfaces mapped by d_{norm}, display individual spikes representing the corresponding interactions, where unique spikes indicate intermolecular interactions. The noticeable marks present on the Hirshfeld surfaces of the complexes are indicative of the contacts Br···H/H···Br (18.4%), O···H/H···O (24.2%), and C···H/H···C (6.6%) for complex **1**, O···H/H···O (32.1%) and C···H/H···C (8.6%) for complex **2**, Cl···H/H···Cl (17.9%), O···H/H···O (22.9%), C···H/H···C (9.4%) and S···H/H···S (3.1%) for complex **3** respectively. The Hirshfeld surface of complex **4** is composed of different proportions of O···H/H···O, C···H/H···C, and S···H/H···S interactions, which account for 23.0%, 7.6%, and 3.9% respectively. The 2D fingerprint plots clearly depict intermolecular interactions in the form of distinct spikes and these are shown in the Fig. 8–11 for complexes **1–4** respectively.

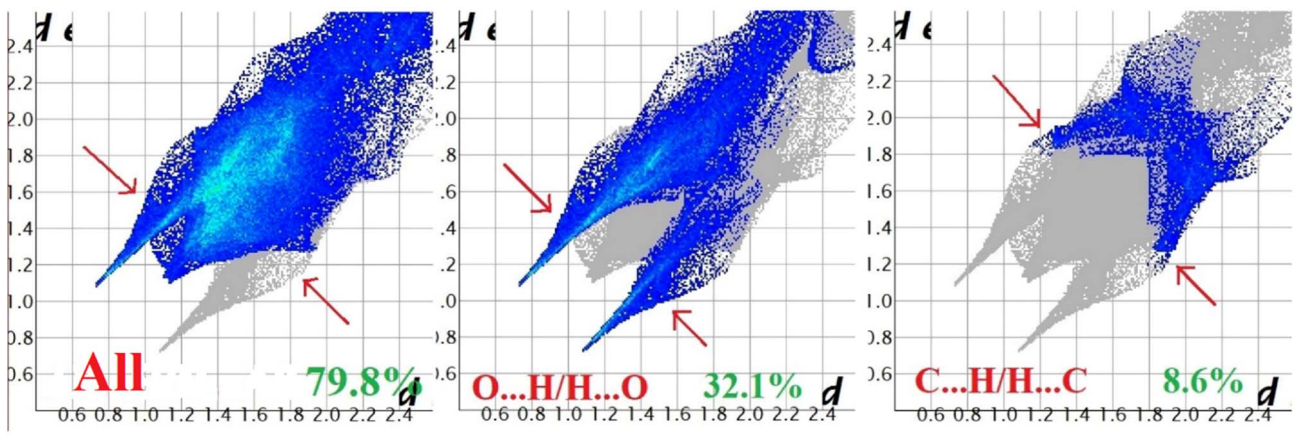

Fig. 9 Fingerprint plot of complex **2**: full and resolved into O···H/H···O, and C···H/H···C contacts contributed to the total Hirshfeld surface area.

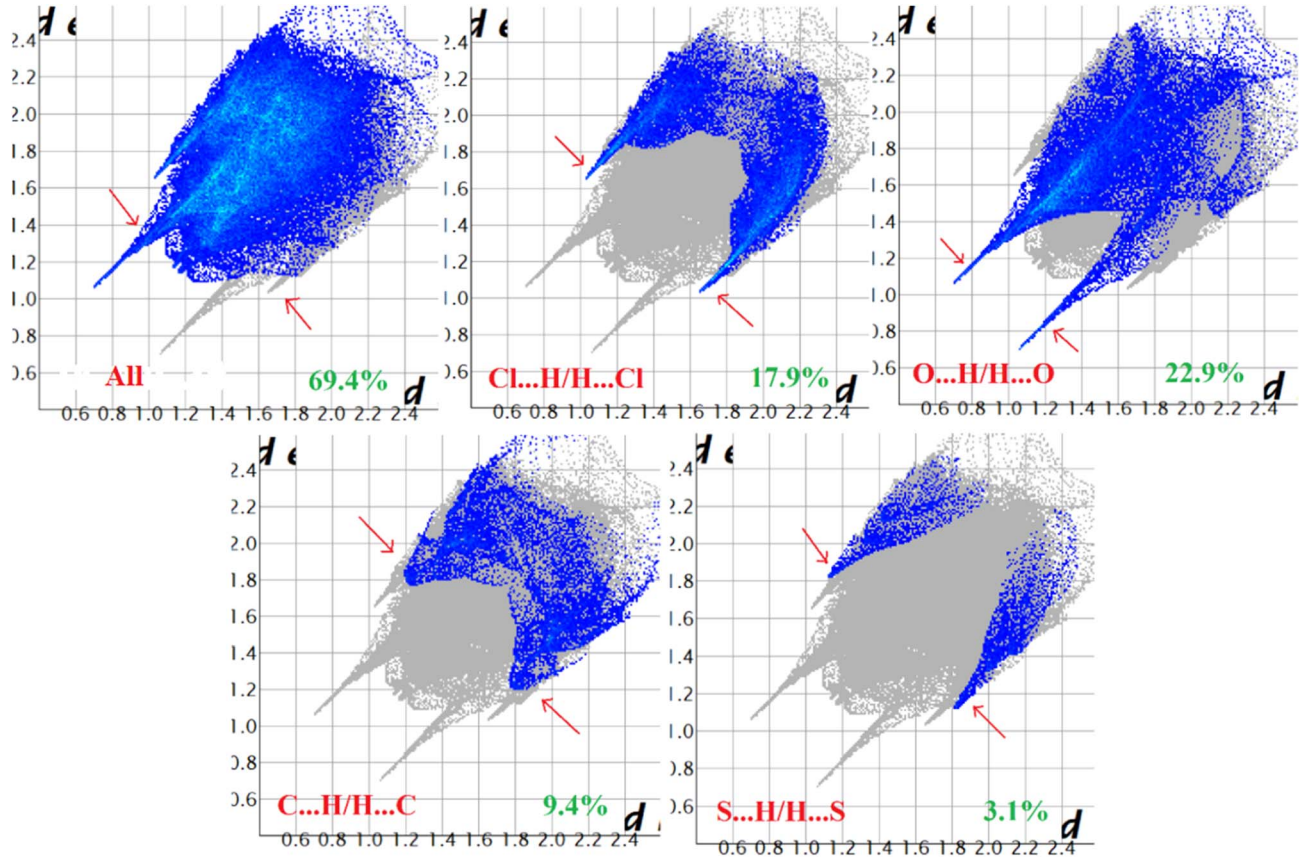

Fig. 10 Fingerprint plot of complex **3**: full and resolved into Cl⋯H/H⋯Cl, O⋯H/H⋯O, C⋯H/H⋯C, and S⋯H/H⋯S contacts contributed to the total Hirshfeld surface area.

IR and electronic spectra and magnetic moment

The IR spectra of complexes **1–4** display consistent and routine observation of broad bands in the 3390–3360 cm^{-1} range due to the existence of coordinated water. All complexes exhibit the presence of the azomethine (C═N) group as indicated by the strong bands around 1608 cm^{-1}. Moreover, the presence of alkyl C–H stretching vibrations is evidenced by the bands appearing within the range 2980–2940 cm^{-1}. Additionally, complexes **1–4** are determined to contain perchlorate ions due to the observation of sharp peaks in the 1080–1040 cm^{-1} range. The IR spectra of all four complexes are shown in Fig. S2–S5 (ESI†) respectively.

Only one symmetric band (corresponding to $^5Tg \leftarrow {}^5Eg$ electronic transition) is expected for the d^4 manganese(III) system under an ideal symmetric octahedral ligand field. However, both static and dynamic Jahn–Teller effects perturb the octahedral symmetry and electronic spectra become complex in nature. In the present case, bands with shoulder have been found around 610–450 nm. The electronic absorption spectra of all four complexes are collected in acetonitrile medium at room temperature. The intense absorption bands in the high energy range of 223–232 nm are ascribed to intra-ligand $\pi \rightarrow \pi^*$ transitions, which include the aromatic rings. The absorption bands around

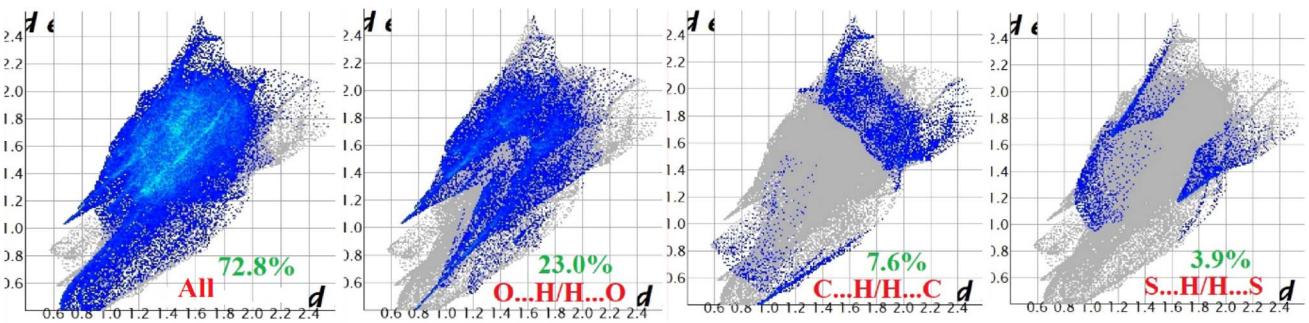

Fig. 11 Fingerprint plot of complex **4**: full and resolved into O⋯H/H⋯O, C⋯H/H⋯C, and S⋯H/H⋯S contacts contributed to the total Hirshfeld surface area.

274–290 nm may be assigned to n → π* transitions within the ligands whereas broad absorption bands have been observed in the lower energy region of 382–393 nm due to ligand-to-metal charge transfer transitions.

The magnetic moment of each complex is ~5.1 B. M. at room temperature. This value is closer to the theoretical value (~4.90 B. M.) for the magnetically isolated high-spin manganese(III) with four unpaired electrons ($S = 2$) with $t_{2g}^3 e_g^1$ electronic configuration.

ESI-MS study

The molecular ion peaks in acetonitrile solution appeared at $m/z = 492.7210$ (theoretical $m/z = 493.06$) for complex **1**, 423.0227 (theoretical $m/z = 423.37$) for complex **2**, 430.9119 (theoretical $m/z = 432.21$) for complex **3** and 439.0023 (theoretical $m/z = 437.35$) for complex **4**. The peaks could correspond to $[Mn(L)]^+$ {L = L^1, L^2, L^3 and L^4 respectively}. The mass spectra of the complexes have been shown in the Fig. S6–S9 (ESI†).

Conclusions

In this work four new manganese(III) complexes have been synthesized and X-ray characterized four manganese(III) complexes with salen type tetradentate N_2O_2 donor Schiff bases. In each of the complexes, the N_2O_2 donor atoms of the salen ligands occupy four equatorial positions of octahedral manganese(III) whereas monodentate ligands (either two water molecules, or one water and one DMSO) occupy two axial sites. In the solid state a recurrent self-assembled motif is observed where the hydrogen-atoms of manganese-coordinated water molecules occupies an electron rich cavity and establish several H-bonds with the oxygen-atoms of the Schiff-base ligands. In addition, concurrent π-stacking interactions are also established, reinforcing the supramolecular complexes. Such assemblies have been analyzed theoretically, including their energetic features and the contribution of the H-bonds. Moreover, as the interactions are established between charged systems, the HaB and ChB interactions observed in the solid state of complexes **1** and **3** have been analyzed using QTAIM and the potential energy density (V_r) predictor, NCIplot and NBO analyses. This method is very useful here, as the interactions are established between charged systems. Conventional procedures based on the supramolecular approach would lead to repulsive cation···cation interactions in **1** and **2** or to very large and attractive interactions for the anion···cation interactions in **3**. The evaluation of the CH···X (X = C, N, S, Cl) contacts using the QTAIM Vr predictor is free from the effect of pure coulombic forces.

Conflicts of interest

The authors declare no conflict of interest.

Acknowledgements

W. S. thanks the CSIR, India, for awarding a Junior Research Fellowship.

References

1 N. Sarkar, M. G. B. Drew, K. Harms, A. Bauzá, A. Frontera and S. Chattopadhyay, *CrystEngComm*, 2018, **20**, 1077–1086.
2 P. Bhowmik, H. P. Nayek, M. Corbella, N. Aliaga-Alcalde and S. Chattopadhyay, *Dalton Trans.*, 2011, **40**, 7916–7926.
3 P. Seth, M. G. B. Drew and A. Ghosh, *J. Mol. Catal. A: Chem.*, 2012, **365**, 154–161.
4 P. Kar and A. Ghosh, *Inorg. Chim. Acta*, 2013, **395**, 67–71.
5 A. Panja, N. Shaikh, M. Ali and P. Banerjee, *Polyhedron*, 2003, **22**, 1191–1198.
6 S. Saha, D. Mal, S. Koner, A. Bhattacherjee, P. Gütlich, S. Mondal, M. Mukherjee and K. Okamoto, *Polyhedron*, 2004, **23**, 1811–1817.
7 M. Karmakar and S. Chattopadhyay, *J. Mol. Struct.*, 2019, **1186**, 155–186.
8 E. Y. Tshuva, I. Goldberg and M. Kol, *J. Am. Chem. Soc.*, 2000, **122**, 10706–10707.
9 H. Kara, *Anal. Sci.*, 2008, **24**, 263–264.
10 M. R. Bermejo, M. I. Fernandez, E. Gomez-Forneas, A. Gonzalez-Noya, M. Maneiro, R. Pedrido and M. J. Rodriguez, *Eur. J. Inorg. Chem.*, 2007, **24**, 3789–3797.
11 I. C. Hwang and K. Ha, *Z. Kristallogr. N. Cryst. Struct.*, 2006, **221**, 363–364.
12 H. Zhou, Y. Wang, X. Shen, Y. Liu and A. Yuan, *Inorg. Chim. Acta*, 2014, **423**, 115–122.
13 X. L. Ma and Z. L. You, *Transition Met. Chem.*, 2008, **33**, 961–965.
14 G. G. Riopedre, M. I. F. Garcia, A. M. G. Noya, M. A. V. Fernandez, M. R. Bermejo and M. Maneiro, *Phys. Chem. Chem. Phys.*, 2011, **13**, 18069–18077.
15 C. G. Zhang, G. H. Tian, Z. F. Ma and D. Y. Yan, *Transition Met. Chem.*, 2000, **25**, 270–273.
16 M. A. V. Fernandez, M. I. F. Garcia, A. M. G. Noya, M. Maneiro, M. R. Bermejo and M. J. R. Douton, *Polyhedron*, 2012, **31**, 379–385.
17 C. H. Li, K. L. Huang, J. M. Dou, Y. N. Chi, Y. Q. Xu, L. Shen, D. Q. Wang and C. W. Hu, *Cryst. Growth Des.*, 2008, **8**, 3141–3143.
18 T. M. Rajendiran, M. T. Caudle, M. L. Kirk, I. Setyawati, J. W. Kampf and V. L. Pecoraro, *J. Biol. Inorg. Chem.*, 2003, **8**, 283–293.
19 T. M. Rajendiran, M. L. Kirk, I. A. Setyawati, M. T. Caudle, J. W. Kampf and V. L. Pecoraro, *Chem. Commun.*, 2003, **82**, 824–825.
20 M. Watkinson, M. Fondo, M. R. Bermejo, A. Sousa, C. A. McAuliffe, R. G. Pritchard, N. Jaiboon, N. Aurangzebc and M. Naeem, *J. Chem. Soc., Dalton Trans.*, 1999, **1**, 31–42.
21 D. Martinez, M. Motevalli and M. Watkinson, *Dalton Trans.*, 2010, **39**, 446–455.
22 K. Ha, *Z. Kristallogr. N. Cryst. Struct.*, 2010, **225**, 257–258.
23 H. Kargar, *Transition Met. Chem.*, 2014, **39**, 811–817.
24 (*a*) A. J. Tasiopoulos, A. Vinslava, W. Wernsdorfer, K. A. Abboud and G. Christou, *Angew. Chem., Int. Ed.*, 2004, **43**, 2117–2121; (*b*) E. C. Sanudo, W. Wernsdorfer, K. A. Abboud and G. Christou, *Inorg. Chem.*, 2004, **43**, 4137–

4144; (*c*) M. Murugesu, J. Raftery, W. Wernsdorfer, G. Christou and E. K. Brechin, *Inorg. Chem.*, 2004, **43**, 4203–4209.
25 (*a*) R. Karmakar, C. R. Choudhury, G. Bravic, J. P. Sutter and S. Mitra, *Polyhedron*, 2004, **23**, 949–954; (*b*) L. Lecren, W. Wernsdorfer, Y. G. Li, A. Vindigni, H. Miyasaka and R. Clerac, *J. Am. Chem. Soc.*, 2007, **129**, 5045–5051.
26 (*a*) A. Daolio, A. Pizzi, M. Calabrese, G. Terraneo, S. Bordignon, A. Frontera and G. Resnati, *Angew. Chem., Int. Ed.*, 2021, **60**, 20723–20727; (*b*) A. Bauza and A. Frontera, *Chem. - Eur. J.*, 2022, **28**, e202201660; (*c*) A. Daolio, A. Pizzi, G. Terraneo, A. Frontera and G. Resnati, *ChemPhysChem*, 2021, **22**, 2281–2285.
27 (*a*) T. Basak, R. M. Gomila, A. Frontera and S. Chattopadhyay, *CrystEngComm*, 2021, **23**, 2703–2710; (*b*) M. Karmakar, A. Frontera, S. Chattopadhyay, T. J. Mooibroek and A. Bauza, *Int. J. Mol. Sci.*, 2020, **21**, 7091; (*c*) S. Roy, M. G. B. Drew, A. Bauza, A. Frontera and S. Chattopadhyay, *New J. Chem.*, 2018, **42**, 6062–6076.
28 S. Thakur, R. M. Gomila, A. Frontera and S. Chattopadhyay, *CrystEngComm*, 2021, **23**, 5087–5096.
29 K. Ghosh, K. Harms, A. Bauza, A. Frontera and S. Chattopadhyay, *CrystEngComm*, 2018, **20**, 7281–7292.
30 S. Thakur, M. G. B. Drew, A. Franconetti, A. Frontera and S. Chattopadhyay, *RSC Adv.*, 2019, **9**, 4789–4796.
31 G. M. Sheldrick, *Acta Crystallogr., Sect. C: Struct. Chem.*, 2015, **71**, 3–8.
32 G. M. Sheldrick, *SADABS, V2014/5, Software for Empirical Absorption Correction*, University of Göttingen, Institute fur Anorganische Chemieder Universitat, Gottingen, Germany, 1999.
33 R. Ahlrichs, M. Bar, M. Haser, H. Horn and C. Kolmel, *Chem. Phys. Lett.*, 1989, **162**, 165–169.
34 A. D. Becker, *Phys. Rev. A*, 1988, **38**, 3098–3100.
35 J. P. Perdew, in *Electronic Structure of Solids '91*, ed. P. Ziesche and H. Eschrig, Akademie Verlag, Berlin, 1991, p. 11.
36 S. Grimme, J. Antony, S. Ehrlich and H. Krieg, *J. Chem. Phys.*, 2010, **132**, 154104.
37 F. Weigend and R. Ahlrichs, *Phys. Chem. Chem. Phys.*, 2005, **7**, 3297–3305.
38 F. Weigend, *Phys. Chem. Chem. Phys.*, 2006, **8**, 1057–1065.
39 R. F. W. Bader, *Chem. Rev.*, 1991, **91**, 893–928.
40 J. C. Garcia, E. R. Johnson, S. Keinan, R. Chaudret, J. P. Piquemal, D. N. Beratan and W. Yang, *J. Chem. Theory Comput.*, 2011, **7**, 625–632.
41 W. Humphrey, A. Dalke and K. Schultan, *J. Mol. Graphics*, 1996, **14**, 33–38.
42 T. Lu and F. Chen, *J. Comput. Chem.*, 2012, **33**, 580–592.
43 E. D. Glendening, C. R. Landis and F. Weinhold, *J. Comput. Chem.*, 2019, **40**, 2234–2241.
44 E. D. Glendening, J. K. Badenhoop, A. E. Reed, J. E. Carpenter, J. A. Bohmann, C. M. Morales, P. Karafiloglou, C. R. Landis and F. Weinhold, *NBO 7.0*. Theoretical Chemistry Institute, University of Wisconsin, Madison, WI. 2018.
45 M. A. Spackman and D. Jayatilaka, *CrystEngComm*, 2009, **11**, 19–32.
46 F. L. Hirshfeld, *Theor. Chim. Acta*, 1977, **44**, 129–138.
47 H. F. Clausen, M. S. Chevallier, M. A. Spackman and B. B. Iversen, *New J. Chem.*, 2010, **34**, 193–199.
48 A. L. Rohl, M. Moret, W. Kaminsky, K. Claborn, J. J. McKinnon and B. Kahr, *Cryst. Growth Des.*, 2008, **8**, 4517–4525.
49 A. Parkin, G. Barr, W. Dong, C. J. Gilmore, D. Jayatilaka, J. J. McKinnon, M. A. Spackman and C. C. Wilson, *CrystEngComm*, 2007, **9**, 648–652.
50 M. A. Spackman and J. J. McKinnon, *CrystEngComm*, 2002, **4**, 378–392.
51 S. K. Wolff, D. J. Grimwood, J. J. McKinnon, D. Jayatilaka and M. A. Spackman, *Crystal explorer 2.0*, University of Western Australia, Perth, 2007, **http://hirshfeldsurfacenet.blogspot.com**.
52 P. Bhowmik, H. P. Nayek, M. Corbella, N. A. Alcalde and S. Chattopadhyay, *Dalton Trans.*, 2011, **40**, 7916–7926.
53 K. Ghosh, S. Banerjee and S. Chattopadhyay, *CrystEngComm*, 2019, **21**, 6859–6868.
54 S. Roy, A. Dey, M. G. B. Drew, P. P. Ray and S. Chattopadhyay, *New J. Chem.*, 2019, **43**, 5020–5031.
55 S. Roy, M. G. B. Drew, A. Bauza, A. Frontera and S. Chattopadhyay, *New J. Chem.*, 2018, **42**, 6062–6076.
56 K. Ghosh, K. Harms, A. Bauzá, A. Frontera and S. Chattopadhyay, *Dalton Trans.*, 2018, **47**, 331–347.
57 X. Yang, R. A. Jones, V. Lynch, M. M. Oye and A. L. Holmes, *Dalton Trans.*, 2005, 849–851.
58 F. Pan, Z. M. Wang and S. Gao, *Inorg. Chem.*, 2007, **46**, 10221–10228.
59 H. Asada, M. Fujiwara and T. Matsushita, *Polyhedron*, 2000, **19**, 2039–2048.
60 F. Z. C. Fellah, J. P. Costes, F. Dahan, C. Duhayon and J. P. Tuchagues, *Polyhedron*, 2007, **26**, 4209–4215.
61 T. Kajiwara, M. Nakano, K. Takahashi, S. Takaishi and M. Yamashita, *Chem. - Eur. J.*, 2011, **17**, 196–205.
62 Y. Yahsi, H. Kara, L. Sorace and O. Buyukgungor, *Inorg. Chim. Acta*, 2011, **366**, 191–197.
63 S. Thakurta, R. J. Butcher, C. J. Gomez-Garcia, E. Garribba and S. Mitra, *Inorg. Chim. Acta*, 2010, **363**, 3981–3986.
64 A. Cucos, A. Ursu, A. M. Madalan, C. Duhayon, J. P. Sutter and M. Andruh, *CrystEngComm*, 2011, **13**, 375–390.
65 S. Rayati, S. Zakavi, M. Koliaei, A. Wojtczak and A. Kozakiewicz, *Inorg. Chem. Commun.*, 2010, **13**, 203–207.
66 N. Sarkar, M. G. B. Drew, K. Harms, A. Bauza, A. Frontera and S. Chattopadhyay, *CrystEngComm*, 2018, **20**, 1077–1086.
67 G. Bhargavi, M. V. Rajasekharan, J. P. Costes and J. P. Tuchagues, *Polyhedron*, 2009, **28**, 1253–1260.
68 K. R. Reddy, M. V. Rajasekharan and J. P. Tuchagues, *Inorg. Chem.*, 1998, **37**, 5978–5982.
69 S. Sen, S. Mitra, D. Luneau, M. S. El Fallah and J. Ribas, *Polyhedron*, 2006, **25**, 2737–2744.
70 D. Cremer and J. A. Pople, *J. Am. Chem. Soc.*, 1975, **97**, 1354–1358.
71 D. Cremer, *Acta Crystallogr., Sect. B: Struct. Sci.*, 1984, **40**, 498–500.
72 J. C. A. Boeyens, *J. Cryst. Mol. Struct.*, 1978, **8**, 317–320.
73 E. V. Bartashevich and V. G. Tsirelson, *Russ. Chem. Rev.*, 2014, **83**, 1181–1203.